18. Scaling analyses, generalizations, and physical consequences appear in the supporting material on *Science* Online.
19. S. Sachdev, K. Park, *Ann. Phys. N.Y.* **298**, 58 (2002).
20. C. Dasgupta, B. I. Halperin, *Phys. Rev. Lett.* **47**, 1556 (1981).
21. A. W. Sandvik, S. Daul, R. R. P. Singh, D. J. Scalapino, *Phys. Rev. Lett.* **89**, 247201 (2002).
22. C. Lhuillier, G. Misguich, http://xxx.lanl.gov/abs/cond-mat/0109146.
23. P. Coleman, C. Pépin, Q. Si, R. Ramazashvili, *J. Phys. Condens. Matt.* **13**, 723 (2001).
24. Q. Si, S. Rabello, K. Ingersent, J. L. Smith, *Nature* **413**, 804 (2001).
25. F. D. M. Haldane, *Phys. Rev.* B **25**, 4925 (1982).
26. B. I. Halperin, T. C. Lubensky, S.-k. Ma, *Phys. Rev. Lett.* **32**, 292 (1974).
27. This research was generously supported by NSF under grants DMR-0213282, DMR-0308945 (T.S.), DMR-9985255 (L.B.), DMR-0098226 (S.S.), and DMR-0210790 and PHY-9907949 (M.P.A.F.). We also acknowledges funding from the NEC Corporation (T.S.), the Packard Foundation (L.B.), the Alfred P. Sloan Foundation (T.S. and L.B.), a Pappalardo Fellowship (A.V.), and an award from The Research Corporation (T.S.). We thank the Aspen Center for Physics for hospitality.

Supporting Online Material
www.sciencemag.org/cgi/content/full/303/5663/1490/DC1
SOM Text
References and Notes

23 September 2003; accepted 7 January 2004

REPORTS

Terahertz Magnetic Response from Artificial Materials

T. J. Yen,[1]* W. J. Padilla,[2]* N. Fang,[1]* D. C. Vier,[2] D. R. Smith,[2] J. B. Pendry,[3] D. N. Basov,[2] X. Zhang[1]†

We show that magnetic response at terahertz frequencies can be achieved in a planar structure composed of nonmagnetic conductive resonant elements. The effect is realized over a large bandwidth and can be tuned throughout the terahertz frequency regime by scaling the dimensions of the structure. We suggest that artificial magnetic structures, or hybrid structures that combine natural and artificial magnetic materials, can play a key role in terahertz devices.

The range of electromagnetic material response found in nature represents only a small subset of that which is theoretically possible. This limited range can be extended by the use of artificially structured materials, or metamaterials, that exhibit electromagnetic properties not available in naturally occurring materials. For example, artificial electric response has been introduced in metallic wire grids or cell meshes, with the spacing on the order of wavelength (*1*); a diversity of these meshes are now used in THz optical systems (*2*). More recently, metamaterials with subwavelength scattering elements have shown negative refraction at microwave frequencies (*3*), for which both the electric permittivity and the magnetic permeability are simultaneously negative. The negative-index metamaterial relied on an earlier theoretical prediction that an array of nonmagnetic conductive elements could exhibit a strong, resonant response to the magnetic component of an electromagnetic field (*4*). In the present work, we show that an inherently nonmagnetic metamaterial can exhibit magnetic response at THz frequencies, thus increasing the possible range in which magnetic and negative-index materials can be realized by roughly two orders of magnitude.

Conventional materials that exhibit magnetic response are far less common in nature than materials that exhibit electric response, and they are particularly rare at THz and optical frequencies. The reason for this imbalance is fundamental in origin: Magnetic polarization in materials follows indirectly either from the flow of orbital currents or from unpaired electron spins. In magnetic systems, resonant phenomena, analogous to the phonons or collective modes that lead to an enhanced electric response at infrared or higher frequencies, tend to occur at far lower frequencies, resulting in relatively little magnetic material response at THz and higher frequencies.

Magnetic response of materials at THz and optical frequencies is particularly important for the implementation of devices such as compact cavities, adaptive lenses, tunable mirrors, isolators, and converters. A few natural magnetic materials that respond above microwave frequencies have been reported. For example, certain ferromagnetic and antiferromagnetic systems exhibit a magnetic response over a frequency range of several hundred gigahertz (*5*–*7*) and even higher (*8*, *9*). However, the magnetic effects in these materials are typically weak and often exhibit narrow bands (*10*), which limits the scope of possible THz devices. The realization of magnetism at THz and higher frequencies will substantially affect THz optics and their applications (*11*).

From a classical perspective, we can view a magnetic moment as being generated by microscopic currents that flow in a circular path. Such solenoidal currents can be induced, for example, by a time-varying magnetic field. Although this magnetic response is typically weak, the introduction of a resonance into the effective circuit about which the current flows can markedly enhance the response. Resonant solenoidal circuits have been proposed as the basis for artificially structured magnetic materials (*12*), although they are primarily envisaged for lower radio-frequency applications. With recent advances in metamaterials, it has become increasingly feasible to design and construct systems at microwave frequencies with desired magnetic and/or electric properties (*3*, *13*, *14*). In particular, metamaterials promise to extend magnetic phenomena because they can be designed to

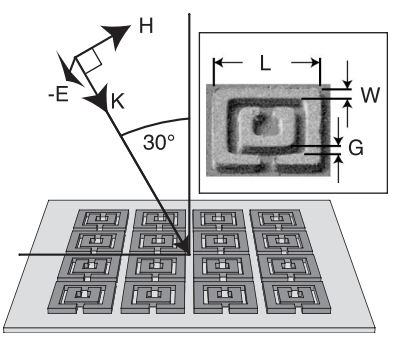

Fig. 1. Illustration depicting the orientation of the 30° ellipsometry experiment. The polarization shown is S-polarization, or transverse electric, for excitation of the magnetic response. P-polarization, transverse magnetic, was also measured. (**Inset**) A secondary ion image of sample D1, taken by focused ion-beam microscopy. For each SRR, the split gap is 2 μm. The corresponding gap between the inner and outer ring (G), the width of the metal lines (W), the length of the outer ring (L), and the lattice parameter were 2, 4, 26, and 36 μm for sample D1; 3, 4, 32, and 44 μm for sample D2, and 3, 6, 36, and 50 μm for sample D3, respectively. These values were used in both design and simulation. K, the wave vector of incident light; H, the magnetic field intensity; –E, the electrical field intensity.

[1]Department of Mechanical and Aerospace Engineering, University of California at Los Angeles, 420 Westwood Plaza, Los Angeles, CA 90095, USA. [2]Department of Physics, University of California, San Diego, 9500 Gilman Drive, La Jolla, CA 92093–0319, USA. [3]Condensed Matter Theory Group, The Blackett Laboratory, Imperial College, London SW7 2AZ, UK.

*These authors contributed equally to this work.
†To whom correspondence should be addressed. E-mail: xiang@seas.ucla.edu

work at high frequencies with broad bandwidth and tunability and can attain large positive or negative values of the magnetic permeability.

A magnetic metamaterial can be formed from an array of nonmagnetic, conducting, split-ring resonators (SRRs) (Fig. 1). An SRR consists of two concentric annuli of conducting material, each with a gap situated oppositely. The gaps enable the structure to be resonant at wavelengths much larger than its physical dimensions, and the combination of many SRRs into a periodic array allows the material to behave as a medium with an effective magnetic permeability $\mu_{eff}(\omega)$, where ω is frequency. The origin of the effective permeability enhancement stems from a resonance in the SRR, associated with the inductance corresponding to the rings and the capacitance corresponding to the gaps within and between the rings.

The effective permeability can be expressed in the form (*4*, *15*)

$$\mu_{eff}(\omega) = 1 - \frac{F\omega^2}{\omega^2 - \omega_0^2 + i\Gamma\omega} = \mu'_{eff}(\omega) + i\mu''_{eff}(\omega) \quad (1)$$

where F is a geometrical factor, ω_0 is the resonance frequency, Γ is the resistive loss in the resonating SRR, and μ'_{eff} and μ''_{eff} are the real and imaginary magnetic permeability functions. In the quasi-static limit, the qualitative picture of this magnetic response is straightforward: The external magnetic field with a varying flux normal to the metallic loop will induce a current flow, which in turn results in a local magnetic dipole moment. Well below the resonance frequency, ω_0, the strength of the magnetic dipole increases with frequency, and this dipole response stays in phase with the excitation field, i.e., it has a paramagnetic response. As the frequency of the incident field approaches ω_0, the currents generated in the loops can no longer keep up with the external field and begin to lag. As the frequency increases above ω_0, the induced dipole moment lags further until it is completely out of phase with the excitation field, which results in a magnetic permeability smaller than unity (i.e., a diamagnetic response), including values less than zero. In contrast to conventional ferromagnetism, the magnetic activity associated with these conductive elements is completely devoid of any permanent magnetic moment.

In order to obtain magnetic resonant behavior in the THz range, the appropriate dimensions of the SRRs can be first approximated by analytical methods (*4*) and then confirmed by numerical simulation. We designed and constructed three different SRR samples on a 400-μm-thick quartz substrate by a self-aligned microfabrication technique called photoproliferated process (*16*). The SRRs are made from copper and are 3 μm thick. Their periodicity is subwavelength (λ/7 in our samples, where λ is the wavelength of the excited field at resonance frequency), which allows the composite to behave as an effective medium to external THz radiation (λ = 300 μm at 1 THz).

Most reported works on microwave metamaterials have focused on characterizing bulk one- and two-dimensional structures, in which waveguide configurations are frequently used. At the submillimeter wavelengths associated with THz frequencies, optical components such as lenses and mirrors are commonly used, making a free-space characterization more convenient to pursue (Fig. 1). We performed the measurements here using spectroscopic ellipsometry at oblique incidence. A Fourier transform infrared spectrometer adapted for S-polarized (Fig. 1) and Ppolarized light from 0.6 THz to 1.8 THz was used for the measurements, with a silicon bolometer as the detector. We placed the sample within an evacuated compartment, then focused light from a mercury arc lamp source on the substrate at an angle of 30° from the surface normal.

In the frequency-dependent ellipsometry measurements (Fig. 2), the parameter plotted, $\tan^{-2}(\Psi)$, represents the inverse absolute square of the ellipsometric parameter $\rho(\omega) = \tan(\Psi)\cdot\exp(i\Delta)$, where Ψ is the amplitude ratio and Δ is the phase difference. This ellipsometric parameter displays the reflectance ratio of two polarizations. The SRRs are expected to respond magnetically when the magnetic field penetrates the rings (S-polarization) (Fig. 1) and to exhibit no magnetic response when the magnetic field is parallel to the plane of the SRR (P-polarization). Thus, the reflectance ratio (Fig. 2) is the natural function to use, because this parameter provides the ratio of the magnetic to electric response from the SRRs (*17*).

The reflectance ratio for sample D1 (Fig. 2, red curve) exhibits a resonant peak, centered at ~1.25 THz in the spectrum. The resonance in the reflectance was broad, nearly 30% of the bandwidth of its center frequency. If the magnetic response was due to the constituent SRRs, then this resonance should scale with dimensions in accordance to Maxwell's equations. In order to elucidate our findings, two more SRRs with different dimensions were characterized (Fig. 2). These SRRs all exhibit a similar magnetic mode, and their resonant frequencies occur between 0.8 and 1.0 THz. We found an expected monotonic redshifting of resonant frequencies as the dimensions of SRRs were scaled up. In addition, the bandwidth of the magnetic response could be tuned by adjusting the parameters of the SRR element.

As further verification that the peaks in Fig. 2 were due to the magnetic response of the SRRs, we performed a numerical simulation using High-Frequency Structure Simulator (HFSS), a commercial electromagnetic mode solver. S-parameter transmission and reflection were calculated as a function of frequency for a periodic infinite array of copper SRRs with the dimensions of the three designed samples (Fig. 2). The calculation was performed to determine the frequency of the resonant magnetic response of the SRRs, for comparison to the ellipsometry measurements (*18*). The results of the simulation and experimental curves were in good agreement. In Fig. 3, we display the simulated real and imaginary portions of the effective magnetic permeability that corresponds to

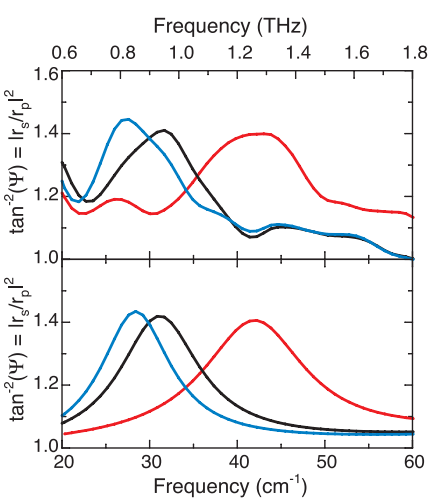

Fig. 2. (**Top**) The ratio of the magnetic to electric response (described in the text) for three different artificial magnetic structures, D1, D2, and D3 (the red, black, and blue solid curves, respectively), in the THz frequency range. (**Bottom**) Theoretical magnetic response, as determined by simulation for each SRR (described in the text). r_s and r_p are the complex reflection coefficients of the S- and P-polarized light.

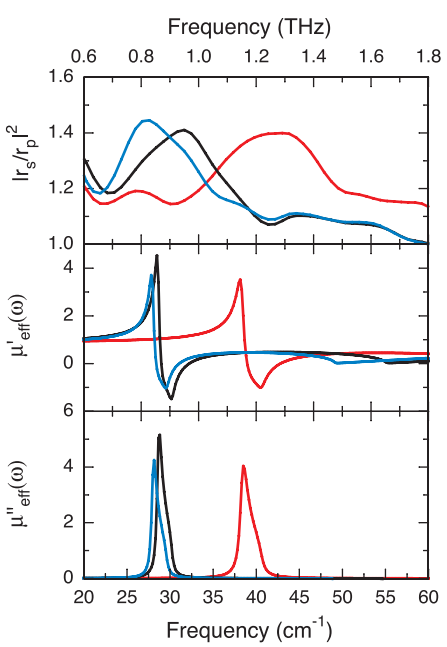

Fig. 3. (**Top**) The ratio of the magnetic to electric response replotted from Fig. 2. Middle and (**bottom**) the real (μ'_{eff}) and imaginary (μ''_{eff}) magnetic permeability functions as simulated by HFSS for samples D1 (red), D2 (black), and D3 (blue).

samples D1, D2, and D3. For sample D1, the onset of the simulated imaginary permeability peak occurs at ~1.15 THz, which corresponds well with the onset of the experimental peak in $\tan^{-2}(\Psi)$. The noticeable difference in the actual peak locations is to be expected, because $\tan^{-2}(\Psi)$ consists of ratios of absolute values; i.e., the resonance width observed is dependent on the strength of the oscillator. Thus, it is important when considering $\tan^{-2}(\Psi)$ and $\mu_{eff}(\omega)$ to compare the onset of the resonances.

The scalability of these magnetic metamaterials throughout the THz range and potentially into optical frequencies promises many applications, such as biological (*19*) and security imaging, biomolecular fingerprinting, remote sensing, and guidance in zero-visibility weather conditions. Additionally, the effect is nearly an order of magnitude larger than that obtained from natural magnetic materials (*20*). Structures with a negative magnetic response, when combined with plasmonic wires that exhibit negative electrical permittivity (*21*–*24*), should produce a negative refractive index material at these very high frequencies, enabling the realization of needed devices in the THz regime.

References and Notes

1. R. Ulrich, *Infrared Phys.* **7**, 37 (1967).
2. S. T. Chase, R. D. Joseph, *Appl. Opt.* **22**, 1775 (1983).
3. R. A. Shelby, D. R. Smith, S. Schultz, *Science* **292**, 79 (2001).
4. J. B. Pendry, A. J. Holden, D. J. Robbins, W. J. Stewart, *IEEE Trans. Microw. Theory Tech.* **47**, 2075 (1999).
5. P. Grunberg, F. Metawe, *Phys. Rev. Lett.* **39**, 1561 (1977).
6. J. R. Sandercock, W. Wettling, *J. Appl. Phys.* **50**, 7784 (1979).
7. R. E. Camley, M. Grimsditch, *Phys. Rev. B* **22**, 5420 (1980).
8. R. E. Camley, D. L. Mills, *Phys. Rev. B* **26**, 1280 (1982).
9. L. Remer, B. Luthi, H. Sauer, R. Geick, R. E. Camley, *Phys. Rev. Lett.* **56**, 2752 (1986).
10. M. R. F. Jensen, S. A. Feiven, T. J. Parker, R. E. Camley, *Phys. Rev. B* **55**, 2745 (1997).
11. C. Sirtori, *Nature* **417**, 132 (2002).
12. I. S. Schelkunoff, H. T. Friis, in *Antennas: Theory and Practice*, S. Sokolnikoff, Ed. (Wiley, New York, 1952), p. 584.
13. D. R. Smith, W. J. Padilla, D. C. Vier, S. C. Nemat-Nasser, S. Schultz, *Phys. Rev. Lett.* **84**, 4184 (2000).
14. C. G. Parazzoli, R. B. Greegor, K. Li, B. E. C. Koltenbah, M. Tanielian, *Phys. Rev. Lett.* **90**, 107401 (2003).
15. S. O'Brien, J. B. Pendry, *J. Phys. Cond. Matter* **14**, 6383 (2002).
16. Materials and methods are available as supporting material on *Science* Online.
17. SRRs also have an electric response in both the P- and S-polarized measurements. This electric contribution is about the same for both polarizations, thus a further advantage of the reflectance ratio measurements is that the electric response is minimized.
18. For ease of calculation and maximum magnetic response, the propagation of the incident radiation was parallel to the plane of the SRRs (90° to the surface normal of Fig. 1). The electrical conductivity used for the copper elements was $\sigma = 5.8 \times 10^7$ S/m; for the quartz substrate, we used a dielectric constant of 3.78. The normal component of effective magnetic permeability $\mu_{eff}(\omega)$ can be extracted from the S-parameter simulation results (*25*) and used to calculate the expected theoretical reflectance ratio $\tan^{-2}(\Psi)$ (Fig. 2, bottom) (*26*).
19. X. C. Zhang, *Phys. Med. Biol.* **47**, 3667 (2002).
20. The individual S- and P-polarization data were fit with the standard Lorentzian form for a resonance. The oscillator strength S can be extracted from the fits, and we found values around $S = 0.6$. This is a large effect in comparison with values we calculated from natural magnetic materials, such as FeF_2, which has a value of $S = 0.07$.
21. D. Wu *et al.*, *Appl. Phys. Lett.* **83**, 201 (2003).
22. S. Gupta, G. Tuttle, M. Sigalas, K. M. Ho, *Appl. Phys. Lett.* **71**, 2412 (1997).
23. J. B. Pendry, A. J. Holden, W. J. Stewart, I. Youngs, *Phys. Rev. Lett.* **76**, 4773 (1996).
24. J. B. Pendry, A. J. Holden, D. J. Robbins, W. J. Stewart, *J. Phys. Cond. Matt.* **10**, 4785 (1998).
25. D. R. Smith, S. Schultz, P. Markoš, C. M. Soukoulis, *Phys. Rev. B* **65**, 195104 (2002).
26. D. Schurig, D. R. Smith, in preparation.

27. We thank Dr. S. Wang for his valuable assistance in analyzing Fourier transform infrared spectra. Supported by the Multidisciplinary University Research Initiative of the U.S. Office of Naval Research/Defense Advanced Research Projects Agency (DARPA) (grant no. N00014-01-1-0803), NSF (grant no. DMI 0216423), and the U.S. Army Research Office/DARPA (grant no. ARO DAAD19-00-1-0525).

Supporting Online Material

www.sciencemag.org/cgi/content/full/303/5663/1494/DC1
Materials and Methods
Figs. S1 and S2

25 November 2003; accepted 5 February 2004

Discovery of Ancient Silicate Stardust in a Meteorite

Ann N. Nguyen* and Ernst Zinner

We have discovered nine presolar silicate grains from the carbonaceous chondrite Acfer 094. Their anomalous oxygen isotopic compositions indicate formation in the atmospheres of evolved stars. Two grains are identified as pyroxene, two as olivine, one as a glass with embedded metal and sulfides (GEMS), and one as an Al-rich silicate. One grain is enriched in ^{26}Mg, which is attributed to the radioactive decay of ^{26}Al and provides information about mixing processes in the parent star. This discovery opens new means for studying stellar processes and conditions in various solar system environments.

Presolar grains were isolated in primitive meteorites only 15 years ago. These grains of stardust formed in the atmospheres of evolved stars and in nova and supernova ejecta. They survived processing in the interstellar medium and in the solar nebula, where most material was heated and homogenized to an average composition. Having undergone minimal alteration, they preserve the original isotopic composition of their parent stars and thus provide important information about stellar evolution and nucleosynthesis. The types of presolar grains identified to date include nanodiamonds; silicon carbide; graphite; silicon nitride; and the oxide grains corundum, spinel, and hibonite (*1*). However, spectroscopic data of young main sequence stars (*2*, *3*) and oxygen-rich asymptotic giant branch stars (AGB) (*4*, *5*) indicate an abundance of submicrometer amorphous silicate grains and crystalline silicate grains of forsterite, enstatite, and diopside. Surprisingly, circumstellar silicate grains were absent from the collection of identified presolar grains despite attempts to isolate them from meteorites (*6*–*8*). The question was whether or not these particles were destroyed by processing in the interstellar medium, solar nebula, or the parent body. A major difficulty in identifying anomalous silicate grains is that the solar system formed under oxidizing conditions and, thus, solar system minerals are dominated by oxidized phases such as oxides and silicates. Consequentially, the identification of a few isotopically anomalous O-rich grains in this great sandbox of oxidized phases of solar system composition requires the analysis of a large number of grains. This difficulty is heightened by the limiting spatial resolution (>1 μm) of the instruments used in previous searches and the expected submicrometer sizes of presolar silicates. Here, we analyzed grains ~100 to 500 nm in size from the primitive meteorite Acfer 094 (*9*) by multidetection raster imaging on the Cameca NanoSIMS, a new type of ion microprobe that affords analysis of submicrometer grains (*9*).

We avoided use of any harsh chemical treatments that may destroy silicate grains and, to reduce the background signal from silicates of solar composition, we only analyzed grains from the matrix, making sure not to break apart any inclusions (*9*). These size-separated grains were dispensed from suspension onto a gold substrate to form a tightly packed layer of grains. Isotopic measurements were performed by obtaining negative secondary ion images of the three O isotopes (^{16}O, ^{17}O, and ^{18}O), ^{24}Mg^{16}O, and ^{28}Si, which were simultaneously detected along with secondary electrons (*9*). These ion images not only allow for the identification of grains with anomalous O isotopic ratios, they also enable the identification of silicate grains using the correlated ^{24}Mg^{16}O and ^{28}Si signals. Because the majority of the grains are of solar system origin and called normal grains hereafter, we used them as standards. A candidate grain was considered presolar if its composition fell well outside of the range for normal grains in the image.

After candidate presolar grains were identified by their oxygen isotopic compositions, we relo-

Laboratory for Space Sciences and the Physics Department, Washington University, St. Louis, MO 63130, USA.

*To whom correspondence should be addressed. E-mail: nguyen@wustl.edu

Terahertz Magnetic Response from Artificial Materials

T. J. Yen *et al.*

Science **303**, 1494 (2004);
DOI: 10.1126/science.1094025